(Received 16 December 2025, Accepted 21 January 2026, Scheduled 9 February 2026)

# A Miniaturized Highly Isolated Quad-Port Penta-Band-Notched UWBMIMO Antenna Based on EBG Structures

Koritala Nagavardhani[1, 2, *], P. Rajesh Kumar[1], and V. Malleswara Rao[1]

[1]*Department of Electronics & Communication Engineering, Andhra University, Visakhapatnam, India*
[2]*Department of Electronics & Communication Engineering, RVR&JC College of Engineering, Guntur, India*

**ABSTRACT:** This paper presents a miniaturized quad-port ultra-wideband (UWB) MIMO antenna that integrates band-notch functionality and exhibits high isolation. The design employed four circular monopole radiators positioned on a modified defected ground structure (DGS) and a periodic electromagnetic bandgap (EBG). These EBG components are an advanced variation of traditional mushroom-type structures that incorporate grid-shaped top patches, a metallic ground plane, and multiple vias connecting both layers. Located at the center of the substrate, the EBG network effectively reduces the electromagnetic coupling between adjacent radiating elements. To achieve multi-band rejection, five inverted U-shaped slots are etched into each monopole, enabling selective suppression of unwanted frequencies at 3.36–3.56 GHz, 3.72–3.92 GHz, 4.11–4.32 GHz, 4.59–4.83 GHz, and 5.22–5.50 GHz, corresponding to WiMAX, C-band, Wi-Fi, INSAT, and WLAN systems. Experimental validation confirms that the antenna attains −10 dB impedance bandwidth extending from 3.0 to 14.0 GHz, with inter-element isolation above −22.5 dB, gain of 6.2 dB, and radiation efficiency reaching 79.2%.

## 1. INTRODUCTION

Ultra-wideband (UWB) communication systems gained regulatory approval following the Federal Communications Commission (FCC) allocation of the 3.1–10.6 GHz spectrum for short-range high-data-rate applications [1]. This opened extensive research into compact UWB antennas suitable for portable wireless devices. Early UWB multiple-input multiple-output (MIMO) antennas were introduced to enhance channel capacity and link reliability; however, strong mutual coupling between closely spaced radiators remained a major limitation. Compact MIMO configurations with enhanced isolation were experimentally demonstrated in [2] and [3], confirming the importance of isolation improvement for practical UWB terminals. Dual-polarized and self-complementary structures were later explored to achieve diversity and band-rejection characteristics [4], while fractal geometries were applied to realize size reduction and WLAN band suppression [5].

To further reduce coupling, several compact two-port and multi-port UWB MIMO designs employing modified ground structures and decoupling techniques were reported in [6–9]. Fundamental antenna design concepts governing impedance matching, radiation, and coupling behavior follow the classical theory outlined in [10]. Parasitic strips and floating decoupling elements were introduced to improve bandwidth and isolation without increasing antenna size [11, 12]. Meanwhile, uniplanar electromagnetic bandgap (EBG) structures exhibiting multiple stopbands were successfully integrated between antenna elements to suppress surface wave coupling [13]. The wave suppression mechanism of EBG structures originates from metamaterial-inspired periodic surfaces initially investigated in [14] and later optimized for coupling reduction in antenna applications [15].

Recent studies have extended UWB MIMO research toward multi-port and multi-band notched antennas. Quad-port and penta-band notched configurations were proposed to mitigate the interference from coexisting wireless systems [16, 17]. Dual-band and triple-band notched UWB-MIMO antennas with high isolation were also reported in [18, 19], demonstrating effective rejection of unwanted bands. Performance evaluation metrics for MIMO antennas, including envelope correlation coefficient and diversity gain, were standardized in [20]. Low-profile UWB MIMO antennas with integrated band rejection were demonstrated in [21], while characteristic mode analysis and neutralization-line loading were applied to improve impedance and isolation performance [22].

Ground-branch protrusion techniques and eye-shaped MIMO structures were introduced to achieve compactness and isolation enhancement [23–25]. Compact diversity antennas employing circular surface plasmon resonance (CSPR) elements and planar extendable arrays were presented in [26, 27], showing scalable MIMO expansion possibilities. Early compact UWB MIMO antennas for portable devices were reported in [28], establishing baseline miniaturization approaches. Moreover, EBG-integrated antenna arrays were originally proposed for the mutual coupling suppression in array environments [29], providing the foundation for modern EBG-based isolation designs.

Although significant progress has been reported on UWB MIMO antennas employing defected ground structures, electromagnetic band-gap surfaces, parasitic elements, and neutral-

* Corresponding author: Koritala Nagavardhani (Koritala.nagavardhani@gmail.com).

ization methods, the majority of existing designs are restricted to two- or three-port configurations and offer limited flexibility in controlling multiple band-notch responses. Quad-port UWB MIMO antennas that simultaneously provide high inter-element isolation, compact physical dimensions, and multiple notch bands are still scarcely investigated in the literature. This research is therefore motivated to address this gap by presenting a miniaturized quad-port UWB MIMO antenna with penta band-notch functionality. The proposed design incorporates EBG structures to improve isolation, suppress unwanted interference, and enable compact integration for next-generation short-range wireless applications. The EBG elements mitigate mutual coupling by inhibiting surface-wave propagation through their intrinsic band-gap characteristics, leading to enhanced isolation between antenna elements. Compared with neutralization lines and defected ground approaches, EBG-based isolation achieves superior decoupling without compromising impedance matching or radiation performance, making it an effective solution for compact multi-port UWB MIMO antenna systems.

This work presents the design and fabrication of a miniaturized UWB-MIMO antenna that integrates multiple band-notch mechanisms and provides low mutual coupling. The baseline element is a circular monopole combined with a modified DGS to cover the full UWB bandwidth. Inverted U-shaped slots etched on the patch generate the required band-stop features. Orthogonal placement of antenna elements reduces coupling for adjacent perpendicular pairs (1–2, 1–4), while a $3 \times 3$ EBG array positioned between parallel elements (1–3, 2–4) significantly enhances isolation. Measurements confirm an operating range of 3.0–14.0 GHz with notch centers at 3.4, 3.8, 4.2, 4.7, and 5.3 GHz, and approximately 22.5 dB isolation between any two ports.

## 2. DESIGN AND ANALYSIS OF ANTENNA

### 2.1. Design Method for Attaining UWB Features

The development process of the proposed UWB antenna system is illustrated in Figure 1. A copper radiating patch with dimensions $27 \times 27 \times 1.6\ \text{mm}^3$ is lithographed on an FR-4 substrate with a dielectric constant of 4.3, a thickness 1.6 mm. The design began with the use of a circular radiator. As seen in Figure 1, this initial version operates at approximately 3.8 GHz and provides a bandwidth of 3 GHz. The rectangular ground plane, with size $W \times L_g$, represents Case I. To widen the bandwidth and meet the UWB requirements, a slot is cut into the ground plane, and its upper corners are removed. These adjustments considerably improve impedance matching and extend the impedance bandwidth from 3.1 GHz to 14.0 GHz. These improved configurations correspond to Cases II and III.

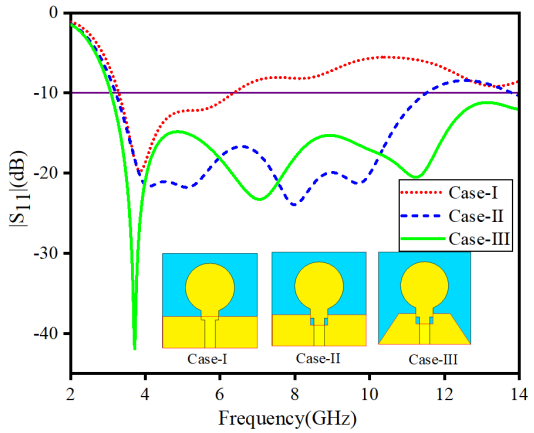


**FIGURE 1**. Simulated reflection coefficient characteristics of different patch antenna configurations.

### 2.2. Procedure for Achieving Notch Band Characteristics

Figure 2 shows that the UWB shares a spectrum with several narrowbands, such as WiMAX, C-band, INSAT, WLAN, X-band, and radio navigation systems, which can cause interference. After confirming the UWB operation of the antenna, notch techniques were introduced to suppress unwanted bands 3.46 GHz (WiMAX), 3.82 GHz (C-band downlink), 4.22 GHz (Wi-Fi), 4.72 GHz (INSAT), and 5.34 GHz (WLAN), as illustrated in Figure 2(a). As depicted in Figure 2(c), the simulated return loss and voltage standing wave ratio (VSWR) confirm five distinct notches within the UWB region, while preserving a broad operating band from 3.0 to 14.0 GHz. The slot dimensions for each rejected band were calculated using the following equations.

$$f_n^i = \frac{c_0}{2L_{slot}^i\sqrt{\varepsilon_{eff}}} \tag{1}$$

$$L_{slot}^i = 2L_i + w_i \tag{2}$$

$$\varepsilon_{eff} = \frac{\varepsilon_r + 1}{2} \tag{3}$$

### 2.3. Parametric Analysis

Figure 3 displays the return loss responses for each suppressed frequency band obtained by modifying the dimensions of respective notch elements. For inverted U-shaped slots, parameters $L_3$ to $L_7$ and $W_3$ to $W_7$ are crucial. At specific frequencies, the currents on the two sides of each slot travel in opposite directions, thereby creating a cancellation effect that produces the corresponding notch band. Figures 3(a)–3(e) illustrate the $S_{11}$ (dB) responses of the proposed UWB antenna, showing five distinct notch bands. These plots reveal that an increase in the total length of a notch structure shifts the stopband to a lower frequency, whereas a reduction in the length pushes it toward higher frequencies. This behavior aligns with Equations (1)–(3), which indicate an inverse relationship between notch length and its corresponding frequency. Moreover, each notch frequency operates independently, allowing precise control over the desired rejection bands by adjusting the dimensions and placement of the notch elements.

### 2.4. Implementation of a Four-Element Antenna Configuration

Figure 4(a) illustrates a four-element UWB-MIMO antenna, where each element occupies $0.072\lambda^2$ and is placed in an orthogonal layout. From the $S$-parameter response, the parallel element pairs (1–3 and 2–4) show an isolation of $-20$ dB

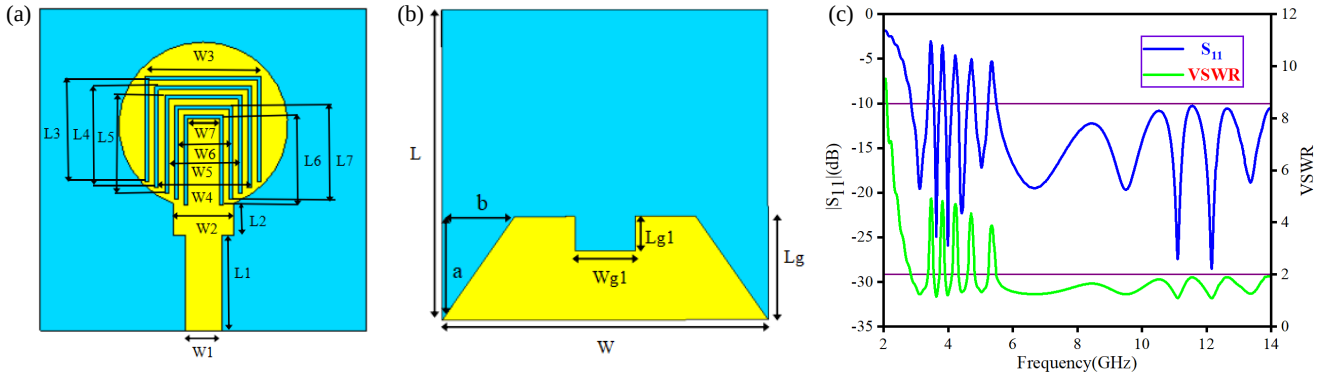


**FIGURE 2**. Structure and dimensions of a single antenna element: (a) Front view, (b) rear view. $R = 7.0$, $W = 27.0$, $W_1 = 3.0$, $W_2 = 5.0$, $W_3 = 9.6$, $W_4 = 8.0$, $W_5 = 6.4$, $W_6 = 4.8$, $W_7 = 3.2$, $W_{g1} = 5.0$, $L = 27.0$, $L_1 = 8.0$, $L_2 = 2.7$, $L_3 = 8.8$, $L_4 = 8.5$, $L_5 = 8.2$, $L_6 = 7.9$, $L_7 = 7.6$, $L_g = 9.0$, $L_g = 9.0$, $L_{g1} = 3.0$, (c) $S_{11}$ and VSWR responses of a single element in the UWB-MIMO antenna configuration.

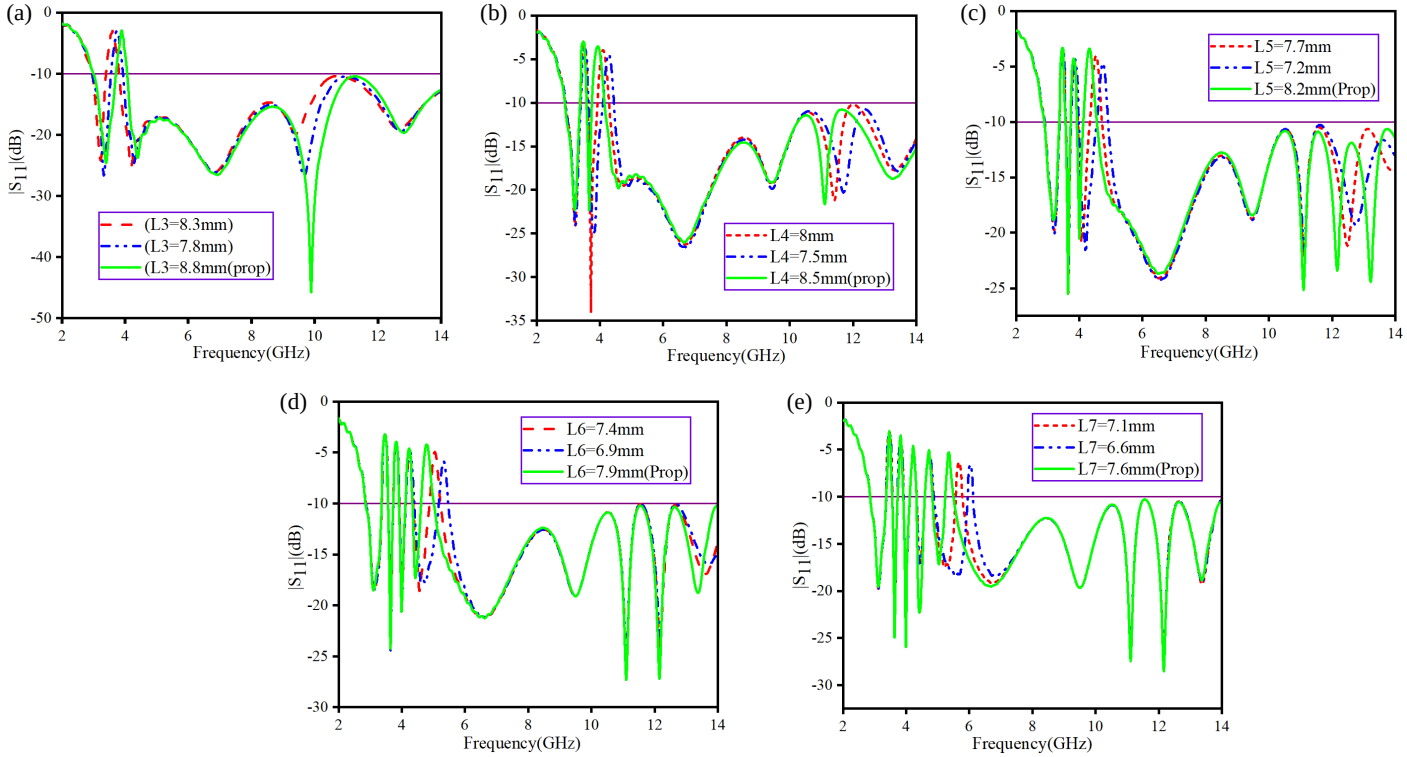


**FIGURE 3**. Simulated $S_{11}$ plots showing variations in (a) the length of the outer slot (slot-1), (b) the length of slot-2, (c) the length of slot-3, (d) the length of slot-4, and (e) the length of the inner slot (slot-5).

only in the 5.0–5.21 GHz to 7.13–8.58 GHz bands. In comparison, the orthogonal pairs (1–2 and 1–4) sustain an isolation of $-22.5$ dB throughout the operating range. The reduced isolation in the parallel elements arises from their similar field distribution and polarization, which increases coupling. To mitigate this, an EBG structure was incorporated.

### 2.5. Analysis of Band-stop Gap Characteristics

EBG structures are well known for creating a band-stop region that suppresses electromagnetic wave propagation between closely spaced antenna elements. To target the coupling observed at 5.0–5.21 GHz and 7.13–8.58 GHz, a periodic $3 \times 3$ EBG array is introduced. Figures 4(b)–4(e) present the array layout, unit cell geometry, design parameters, and corresponding LC-based equivalent circuit. The behavior of the EBG can be interpreted through this resonant LC model, where $C_1$ arises from the fringing capacitance between neighboring cells; $C_2$ represents the capacitance between the patch and the ground plane through the dielectric layer; and $L$ is the contribution of the metallic vias. For a unit cell characterized by the patch width ($W$), gap ($g$), substrate height ($h$), and dielectric constant ($\varepsilon_r$), the values of $L$, $C_1$, and $C_2$ were obtained using the relations provided below.

$$c_1 = \frac{\varepsilon_0 w}{\pi} \text{arch}\left(\frac{w+g}{g}\right) \tag{4}$$

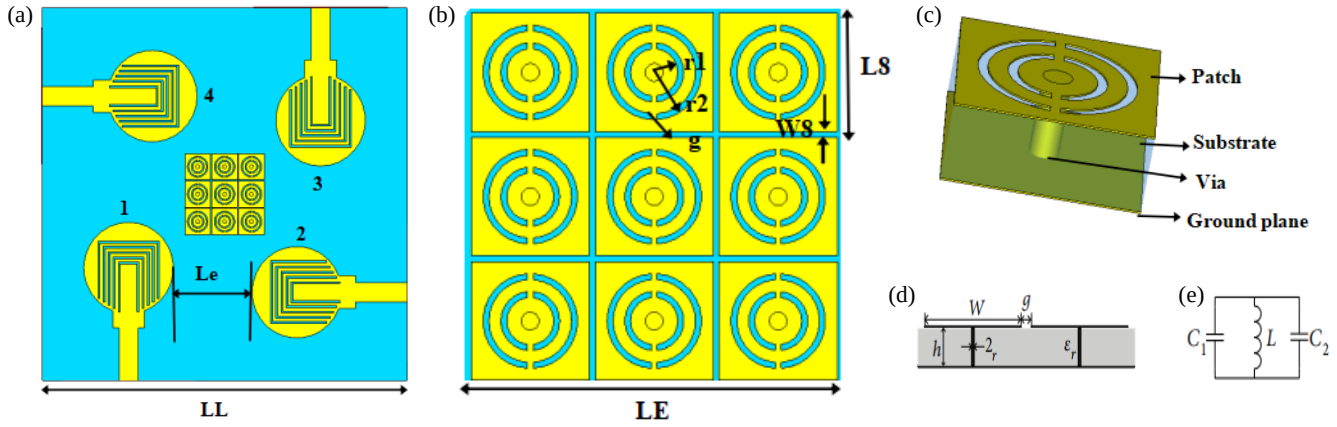


**FIGURE 4**. (a) Structure and dimensions of the four-port UWB-MIMO antenna. (b) Configuration of the $3 \times 3$ EBG array. (c) Layout of a single unit cell. (d) Dimensional details of the unit cell. (e) Corresponding equivalent parallel LC resonance circuit. All dimensions are in millimeters: $LL = 54$, $L_e = 15.3$, $W_8 = 4$, $L_8 = 4$, $g = 0.2$, $LE = 12.4$, $h = 1.6$, $r_1 = 0.8$, and $r_2 = 1.6$.

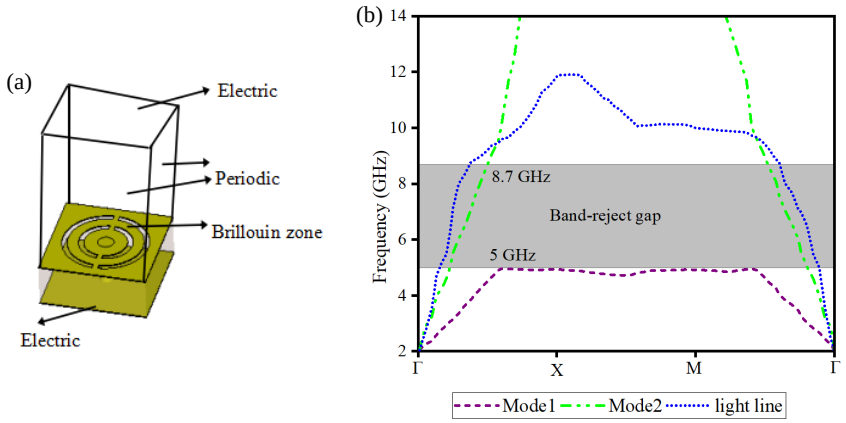


**FIGURE 5**. Band-stop characteristics of the mushroom-shaped EBG structure. (a) Unit cell configuration in CST MWS. (b) Simulated surface wave band diagram of the unit cell.

$$c_2 = \frac{\varepsilon_0 \varepsilon_r w'}{\pi} \text{arch}\left(\frac{\sinh\left(\pi\left(w'+g\right)/4h\right)}{\sinh\left(\pi g/4h\right)}\right) \quad (5)$$

$$L = \mu_0 h \left\{\frac{1}{\pi}\left[\ln\left(\frac{a+\sqrt{a^2-(2r)^2}}{2r}\right)+\ln 2^{1/2}\right]\right\} \quad (6)$$

$$f_0 = \frac{1}{2\pi\sqrt{LC}} \quad (7)$$

where $w' \approx (1{-}2S/W^2)W$, $S = \pi r^2$, $a = W + g$, $C = C_1 + C_2$, where $S$ represents the cross-sectional area of via hole; $\mu_0$ is the permeability of free space; and $\varepsilon_0$ is the permittivity of free space. The initial unit cell parameters are computed using Equations (4)–(7) based on the target frequency bands of 5.0–5.21 GHz and 7.13–8.58 GHz.

A dispersion diagram was generated to examine the high-impedance characteristics of the EBG structure. Based on the initial parameters, the surface wave propagation within the EBG unit cell was analyzed. The side walls were assigned periodic boundary conditions, while the top and bottom surfaces were treated as perfect conductors, as depicted in Figure 5(a). The optimized EBG unit cell dimensions were set to $r_1 = 0.8$ mm, $r_2 = 1.6$ mm, $W = 4.0$ mm, and $g = 0.2$ mm to cover 5.0–5.21 GHz and 7.13–8.58 GHz frequency bands. The dispersion ($k$-$\beta$) characteristics of the surface modes were obtained as shown in Figure 5(b). A distinct band-stop region between the first (TM0) and second (TE1) modes was observed across 5.0–8.58 GHz. In this context, $\Gamma$, $X$, and $M$ represent symmetry points within the irreducible Brillouin zone, where $\Gamma$-$X$ corresponds to $\beta_x a/\pi$ at $\beta_x = 0$; $X$-$M$ corresponds to $\beta_x a/\pi$ at $\beta_x = \pi/a$; and $M$-$\Gamma$ corresponds to $\beta_x a/\pi$ when $\beta_x = \beta_x$ [11–14]. Considering the slow-wave propagation characteristics of the surface modes, the dispersion curves lie below the light lines. The band-stop region extending from 5.0 to 8.58 GHz enhances the isolation between parallel antenna elements from 20 dB to 22.5 dB when a $3 \times 3$ EBG array is placed at the center of the substrate, as illustrated in Figure 6(a).

## 3. RESULTS AND DISCUSSION

Key performance metrics, including $S$-parameters, gain, and radiation patterns, were evaluated using an Anritsu vector network analyzer covering 5 kHz–15 kHz range. The far-field characteristics of the antenna were further examined in an ane-

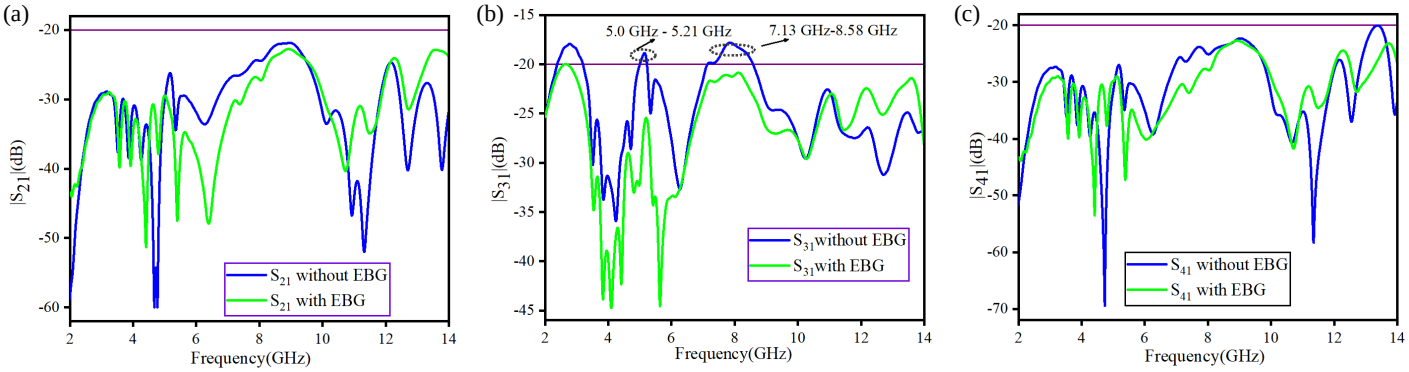


**FIGURE 6**. Comparison of simulated isolation levels with and without the inclusion of EBG structures. (a) $S_{31}$, (b) $S_{21}$, (c) $S_{41}$.

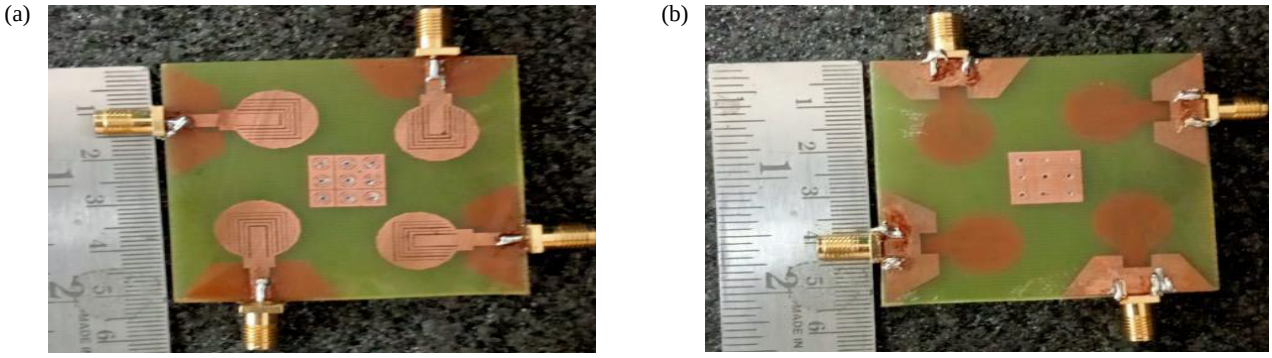


**FIGURE 7**. Prototype model. (a) Front view. (b) Back view.

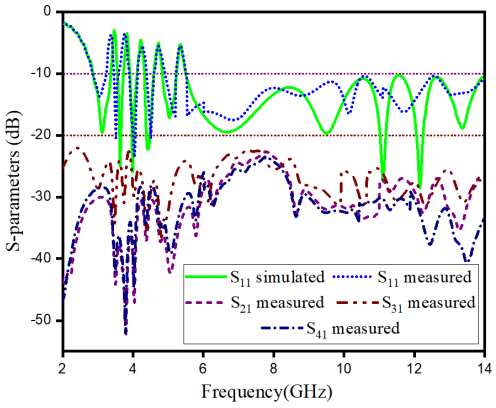


**FIGURE 8**. $S$-parameters.

choic chamber over 20 kHz–20 GHz. Electromagnetic analyses were performed using Computer Simulation Technology (CST) Microwave Studio, and Figure 7 shows the fabricated prototype.

Figure 8 shows that the suggested antenna achieves 3.0–14.0 GHz impedance bandwidth with five notched bands that suppress WiMAX, C-band, Wi-Fi, INSAT, and WLAN interference.

The isolation behavior of the UWB-MIMO antenna was evaluated using $S$-parameters ($S_{21}$, $S_{31}$, and $S_{41}$). As depicted in Figure 8, the simulated and experimental results lie below $-22.5$ dB across the operating bandwidth. Minor discrepancies between the simulated and experimental outcomes were incorporated, accounting for fabrication tolerances, the influence of SMA connectors and soldering, variations in the substrate's dielectric constant, and imperfections in the measurement setup.

### 3.1. The Gain and Radiation Patterns

Figure 9 illustrates the radiation performance of the antenna in the $E$-plane and $H$-plane at representative frequencies of 4 GHz, 7 GHz, and 10 GHz. At these designated frequencies, the co-polarized components in the $E$-plane exhibit two dominant beams oriented in the broadside directions around $(-75°, 80°)$ and $(105°, 260°)$, where the cross-polarized components remain comparatively weak. The co- and cross-polarization difference in the broadside direction exceeded 15 dB, confirming the strong $E$-plane radiation performance. In the $H$-plane, the co-polarized radiation maintains an almost omnidirectional pattern, with the cross-polarized components remaining consistently low across all three frequencies. The polarization isolation in this plane is greater than 20 dB, reflecting a stable and well-balanced radiation behavior.

Figure 10 illustrates both the simulated and measured peak gain values, which show strong consistency. Across the impedance bandwidth of 3.0–14.0 GHz, gain varies from 1.00 dB to 4.10 dB, excluding the notched bands. At lower frequencies (3.0–4.5 GHz), the gain remained relatively low owing to the compact size of a single radiating element.

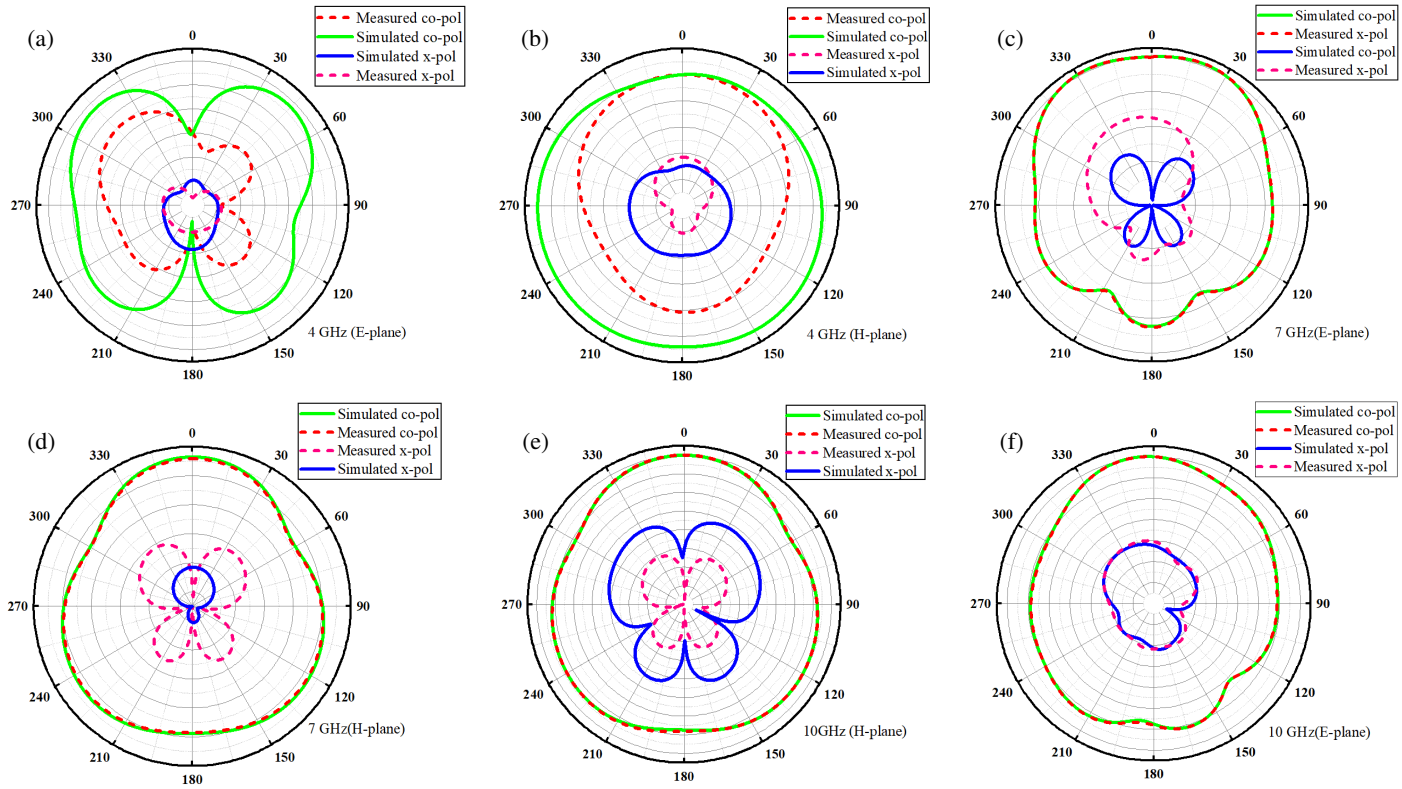


**FIGURE 9**. Radiation patterns at 4 GHz, 7 GHz, and 10 GHz.

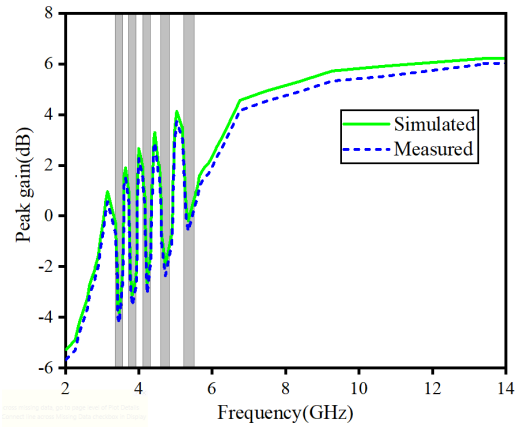


**FIGURE 10**. Peak gain of the suggested antenna.

However, as the frequency increases from 6.0 to 14.0 GHz, the gain increases significantly.

### 3.2. Diversity Characteristics

The performance of MIMO antennas is typically assessed using several key parameters, including envelope correlation coefficient (ECC), diversity gain (DG), radiation efficiency, channel capacity loss (CCL), and total active reflection coefficient (TARC). ECC measures the correlation level between antenna elements, and a lower ECC value signifies a superior diversity performance. For an optimal operation, ECC should remain below 0.5, ensuring minimal signal correlation. In multi-port MIMO configurations, ECC (represented as $\rho_{eij}$) is derived from the simulated 3D radiation patterns as

$$\rho_{eij} = \frac{\left|\int_0^{2\pi}\int_0^{\pi}\left(XPRE_{\theta i}E^*_{\theta j}P_\theta + E_{\varphi i}E^*_{\varphi j}P\varphi\right)d\Omega\right|^2}{\int_0^{2\pi}\int_0^{\pi}\left(XPRE_{\theta i}E^*_{\theta i}P_\theta + E_{\varphi i}E^*_{\varphi i}P\varphi\right)d\Omega \times \int_0^{2\pi}\int_0^{\pi}\left(XPRE_{\theta j}E^*_{\theta j}P_\theta + E_{\varphi j}E^*_{\varphi j}P\varphi\right)d\Omega} \tag{8}$$

Diversity gain (DG) is determined using an equation that represents the antenna's capability to preserve signal quality over multiple propagation paths.

$$DG = 10\sqrt{1 - ECC^2} \tag{9}$$

Figure 11(a) illustrates the ECC and DG of the proposed UWB-MIMO antenna system. The ECC remains below 0.02 throughout the UWB, except at the designated notch frequencies. Even in these notched regions, ECC was below 0.05. Moreover, the antenna achieves a diversity gain (DG) higher than 9.5 dBi across the operational band, apart from three notched segments, confirming its ability to maintain low correlation and strong diversity performance. Figure 11(b) depicts the radiation efficiency, showing a maximum value of 79.2% at 10 GHz, further indicating robust diversity behavior. The total active reflection coefficient (TARC) expresses the effective return loss for the MIMO antenna system [23]. In MIMO applications, the optimal channel capacity loss (CCL) is typically less than 0 dB. As shown in Figure 11(c), the TARC remains below $-10$ dB across the operating band, except at the notch frequencies.

**TABLE 1**. Comparison to prior existing designs.

| Ref. | Antenna size ($mm^2$) | Bandwidth (GHz) | Gain (dB) | Isolation (dB) | ECC | CCL (bbs/Hz) | TARC (dB) | No. of notches | No. of ports |
|---|---|---|---|---|---|---|---|---|---|
| [9] | $80 \times 80$ | 3–14 | 4.8 | $> 20$ | $< 0.02$ | $< 0.3$ | $< -13$ | 5 | 4 |
| [17] | $24 \times 40$ | 2.9–12 | 5.0 | $> 23$ | $< 0.2$ | NA | $< -12$ | 4 | 2 |
| [19] | $39 \times 39$ | 2.3–13.75 | 4.6 | $> 22$ | $< 0.02$ | $< 0.2$ | $< -10$ | 3 | 4 |
| [21] | $30 \times 30$ | 3.1–11.0 | 5.0 | $> 20$ | $< 0.02$ | $< 0.35$ | $< -10$ | 1 | 2 |
| [22] | $24 \times 31$ | 3.4–12.1 | 4.4 | $> 16$ | $< 0.001$ | NA | $< -10$ | 2 | 2 |
| [25] | $34 \times 18$ | 2.93–20.0 | 7.0 | $> 22$ | $< 0.01$ | NA | $< -20$ | 2 | 2 |
| [26] | $23 \times 29$ | 3–12 | 5.9 | $> 15$ | $< 0.15$ | NA | NA | NA | 2 |
| [27] | $38 \times 38$ | 3.0–15.0 | 5.0 | $> 15$ | $< 0.15$ | $< 0.4$ | NA | NA | 4 |
| [28] | $40 \times 26$ | 2.9–12.0 | 6.5 | $> 15$ | $< 0.2$ | NA | NA | NA | 2 |
| [29] | $30 \times 30$ | 3.08–10.98 | 5 | $> 20$ | $< 0.013$ | $< 0.35$ | $< -10$ | 1 | 2 |
| This work | $54 \times 54$ | 3.0–14.0 | 6.2 | $> 22.5$ | $< 0.02$ | $< 0.2$ | $< -10$ | 5 | 4 |

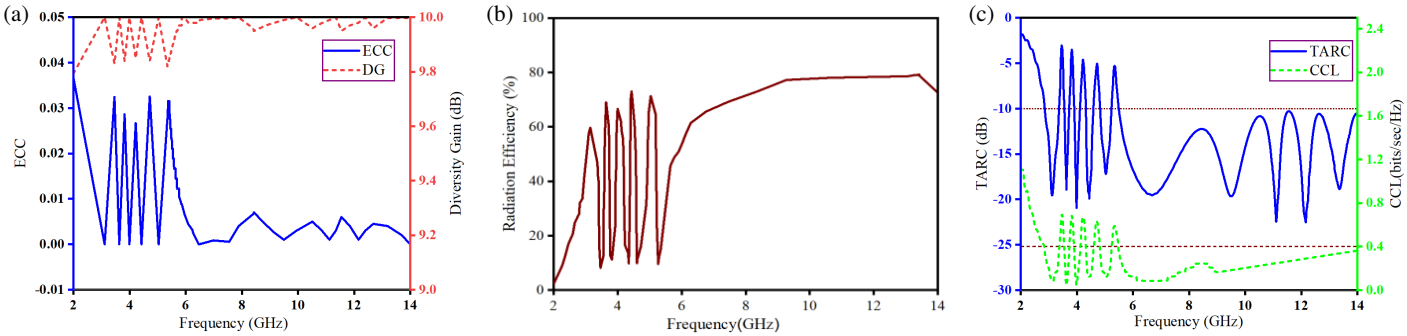


**FIGURE 11**. (a) ECC and DG. (b) Radiation efficiency. (c) The CCL and TARC.

### 3.3. Performance Comparison

Table 1 presents a comparative overview of the suggested design along with several recently published UWB-MIMO antennas. The results indicate that the proposed antenna offers a well-balanced combination of features, including compact size, wide operating bandwidth, improved gain, stable radiation, strong isolation, and excellent MIMO diversity performance (ECC, gain, CCL, and TARC).

## 4. CONCLUSION

This work presents a miniaturized penta-band suppressed quad-port UWB-MIMO antenna system with improved isolation achieved through the integration of EBG structures. The suggested antenna, with a compact footprint of $54 \times 54 \times 1.6\,mm^3$, operates across a broad 3–14 GHz range while simultaneously suppressing interference at 3.46, 3.82, 4.22, 4.72, and 5.34 GHz corresponding to the WiMAX, C-band, Wi-Fi, INSAT, and WLAN bands. The orthogonal arrangement of the radiating elements, combined with EBG structures, significantly enhances isolation. A comprehensive evaluation of diversity performance indicators, including radiation efficiency, ECC, TARC, DG, and CCL, validates the operational characteristics of the antenna. In summary, the proposed quad-element UWB-MIMO antenna system exhibited excellent band-rejection capability and high isolation.

The proposed miniaturized quad-port penta-band-notched UWB MIMO antenna is well-suited for short-range high-data-rate wireless communication systems, including indoor UWB-based data transmission and device-to-device connectivity. The integrated band-notch characteristics enable reliable operation in environments containing coexisting WLAN, WiMAX, and 5G sub-6 GHz services, thereby reducing electromagnetic interference. Owing to its compact size and high isolation, the antenna is appropriate for portable and wearable electronic devices, such as smart sensors, healthcare monitoring units, and internet of things (IoT) terminals.

## REFERENCES

[1] FCC, "Revision of part 15 of the commission's rules regarding ultra-wideband transmission systems," First Report and Order, ET Docket 98-153, 2002.

[2] Khan, M. K., Q. Feng, and Z. Zheng, "Experimental investigation and design of UWB MIMO antenna with enhanced isolation," *Progress In Electromagnetics Research C*, Vol. 107, 287–297, 2021.

[3] Ali, W. A. E. and A. A. Ibrahim, "A compact double-sided MIMO antenna with an improved isolation for UWB applications," *AEU — International Journal of Electronics and Communications*, Vol. 82, 7–13, 2017.

[4] Zhu, J., S. Li, B. Feng, L. Deng, and S. Yin, "Compact dual-polarized UWB quasi-self-complementary MIMO/diversity antenna with band-rejection capability," *IEEE Antennas and Wireless Propagation Letters*, Vol. 15, 905–908, 2016.

[5] Tripathi, S., A. Mohan, and S. Yadav, "A compact Koch fractal UWB MIMO antenna with WLAN band-rejection," *IEEE Antennas and Wireless Propagation Letters*, Vol. 14, 1565–1568, 2015.

[6] Urimubenshi, F., D. B. O. Konditi, J. de Dieu Iyakaremye, P. M. Mpele, and A. Munyaneza, "A novel approach for low mutual coupling and ultra-compact two port MIMO antenna development for UWB wireless application," *Heliyon*, Vol. 8, No. 3, e09057, 2022.

[7] Khan, M. K. and Q. Feng, "Design validation of UWB MIMO antenna with enhanced isolation and novel strips for stop-band characteristics," *Entropy*, Vol. 24, No. 6, 766, 2022.

[8] Navarro-Peralta, A. N., G. Leija-Hernández, and L. A. Iturri-Hinojosa, "Mutual coupling reduction between elements of UWB MIMO antenna using DGS enhancing the impedance bandwidth," in *2023 IEEE International Autumn Meeting on Power, Electronics and Computing (ROPEC)*, 1–6, Ixtapa, Mexico, 2023.

[9] Babu, S. R. and P. Dinesha, "Design of penta-band notched UWB MIMO antenna for diverse wireless applications," *Progress In Electromagnetics Research M*, Vol. 107, 35–49, 2022.

[10] Balanis, C. A., *Antenna Theory: Analysis and Design*, Chap. 14, 811–872, John Wiley & Sons, 2005.

[11] Ding, K., C. Gao, D. Qu, and Q. Yin, "Compact broadband MIMO antenna with parasitic strip," *IEEE Antennas and Wireless Propagation Letters*, Vol. 16, 2349–2353, 2017.

[12] Khan, M. S., A.-D. Capobianco, A. I. Najam, I. Shoaib, E. Autizi, and M. F. Shafique, "Compact ultra-wideband diversity antenna with a floating parasitic digitated decoupling structure," *IET Microwaves, Antennas & Propagation*, Vol. 8, No. 10, 747–753, Jul. 2014.

[13] Dabas, T., D. Gangwar, B. K. Kanaujia, and A. K. Gautam, "Mutual coupling reduction between elements of UWB MIMO antenna using small size uniplanar EBG exhibiting multiple stop bands," *AEU — International Journal of Electronics and Communications*, Vol. 93, 32–38, 2018.

[14] Markley, L. and G. V. Eleftheriades, "A negative-refractive-index metamaterial for incident plane waves of arbitrary polarization," *IEEE Antennas and Wireless Propagation Letters*, Vol. 6, 28–32, 2007.

[15] Assimonis, S. D., T. V. Yioultsis, and C. S. Antonopoulos, "Computational investigation and design of planar EBG structures for coupling reduction in antenna applications," *IEEE Transactions on Magnetics*, Vol. 48, No. 2, 771–774, 2012.

[16] Saritha, V., V. N. K. R. Devana, M. B. Lakshmi, M. A. Halimi, G. Devi, N. R. Lavuri, and A. J. A. Al-Gburi, "Low-profile four-port MIMO antenna realizing penta-band notches for UWB systems," *Optik*, Vol. 336, 172454, 2025.

[17] Babu, S. R. and P. Dinesha, "Design and development of a miniaturized highly isolated UWB-MIMO diversity antenna with quad band notch characteristics," *Progress In Electromagnetics Research C*, Vol. 131, 197–208, 2023.

[18] Eltrass, A. S. and N. A. Elborae, "New design of UWB-MIMO antenna with enhanced isolation and dual-band rejection for WiMAX and WLAN systems," *IET Microwaves, Antennas & Propagation*, Vol. 13, No. 5, 683–691, 2019.

[19] Tang, Z., X. Wu, J. Zhan, S. Hu, Z. Xi, and Y. Liu, "Compact UWB-MIMO antenna with high isolation and triple band-notched characteristics," *IEEE Access*, Vol. 7, 19 856–19 865, 2019.

[20] Abbas, A., N. Hussain, M. A. Sufian, J. Jung, S. M. Park, and N. Kim, "Isolation and gain improvement of a rectangular notch UWB-MIMO antenna," *Sensors*, Vol. 22, No. 4, 1460, 2022.

[21] Biswal, S. P. and S. Das, "A low-profile dual port UWB-MIMO/diversity antenna with band rejection ability," *International Journal of RF and Microwave Computer-Aided Engineering*, Vol. 28, No. 1, e21159, 2018.

[22] Kumar, P., T. Ali, and M. P. Mm, "Characteristic mode analysis-based compact dual band-notched UWB MIMO antenna loaded with neutralization line," *Micromachines*, Vol. 13, No. 10, 1599, 2022.

[23] Mchbal, A., N. A. Touhami, H. Elftouh, and A. Dkiouak, "Mutual coupling reduction using a protruded ground branch structure in a compact UWB owl-shaped MIMO antenna," *International Journal of Antennas and Propagation*, Vol. 2018, No. 1, 4598527, Sep. 2018.

[24] Chandel, R., A. K. Gautam, and K. Rambabu, "Design and packaging of an eye-shaped multiple-input–multiple-output antenna with high isolation for wireless UWB applications," *IEEE Transactions on Components, Packaging and Manufacturing Technology*, Vol. 8, No. 4, 635–642, Apr. 2018.

[25] Chandel, R., A. K. Gautam, and K. Rambabu, "Tapered fed compact UWB MIMO-diversity antenna with dual band-notched characteristics," *IEEE Transactions on Antennas and Propagation*, Vol. 66, No. 4, 1677–1684, Apr. 2018.

[26] Khan, M. S., A.-D. Capobianco, S. M. Asif, D. E. Anagnostou, R. M. Shubair, and B. D. Braaten, "A compact CSRR-enabled UWB diversity antenna," *IEEE Antennas and Wireless Propagation Letters*, Vol. 16, 808–812, 2016.

[27] Sipal, D., M. P. Abegaonkar, and S. K. Koul, "Easily extendable compact planar UWB MIMO antenna array," *IEEE Antennas and Wireless Propagation Letters*, Vol. 16, 2328–2331, 2017.

[28] Liu, L., S. W. Cheung, and T. I. Yuk, "Compact MIMO antenna for portable devices in UWB applications," *IEEE Transactions on Antennas and Propagation*, Vol. 61, No. 8, 4257–4264, Aug. 2013.

[29] Yang, F. and Y. Rahmat-Samii, "Microstrip antennas integrated with electromagnetic band-gap (EBG) structures: A low mutual coupling design for array applications," *IEEE Transactions on Antennas and Propagation*, Vol. 51, No. 10, 2936–2946, 2003.